Modeling of bond behavior of hybrid rods for concrete reinforcement

Antonio Nanni† and Judy Liu‡

Department of Architectural Engineering, The Pennsylvania State University, University Park, PA, 16802, U.S.A.

Abstract. Fiber reinforced plastic (FRP) rods are used as reinforcement (prestressed or not) to concrete. FRP composites can also be combined with steel to form hybrid reinforcing rods that take advantage of the properties of both materials. In order to effectively utilize these rods, their bond behavior with concrete must be understood. The objective of this study is to characterize and model the bond behavior of hybrid FRP rods made with epoxy-impregnated aramid or poly-vinyl alcohol FRP skins directly braided onto a steel core. The model closely examines the split failure of the concrete by quantifying the relationship between slip of the rods resulting transverse stress field in concrete. The model is used to derive coefficients of friction for these rods and, from these, their development length requirements. More testing is needed to confirm this model, but in the interim, it may serve as a design aide, allowing intelligent decisions regarding concrete cover and development length. As such, this model has helped to explain and predict some experimental data from concentric pull-out tests of hybrid FRP rods.

Key words: bond; concrete; concrete cover; development length; fiber reinforced plastic (FRP); friction; hybrid reinforcement; modeling; pull-out test.

1. Introduction

Bond of fiber reinforced plastic (FRP) reinforcement to concrete is of great interest for several reasons. First, the bond mechanism affects the structural performance of any reinforced concrete (RC) member (i.e., the stress in the reinforcement at the crack interface is controlled by bond as is the crack opening width and the crack spacing). Second, the bond mechanism determines the anchorage requirements (i.e., development length) and, to an extent, the thickness of concrete cover. Third, the bond mechanism of FRP to concrete is rod type dependent (i.e., FRP reinforcement can be produced with different external configurations, using different constituent materials in different proportions, and can be manufactured according to different technologies). This last point may be an unpleasant revelation to designers in the construction industry as it may not be possible to generalize results obtained with a specific product.

With respect to bond mechanism, the single most important difference between conventional steel reinforcing bars and FRP rods relates to the anisotropy and heterogeneity of the latter. Elastic modulus, Poisson's ratio, coefficient of thermal expansion, and other mechanical parameters are different in the longitudinal and transvers directions. Longitudinal properties are controlled by fibers, whereas transverse properties are controlled by resin (Mallik 1988). From this it derives that, for example, the shear modulus is not directly related to the elastic modulus. Furthermore, material heterogeneity couples with that resulting from combined manufacturing. For example,

---

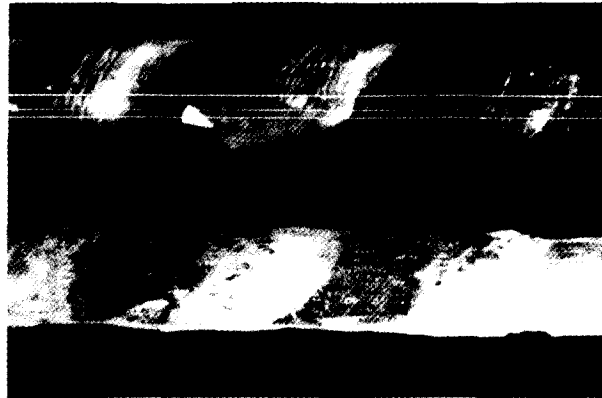† Professor
† Research Assistant

Fig. 1 Pultruded glass FRP rod before (top) and after (bottom) pull-out test.
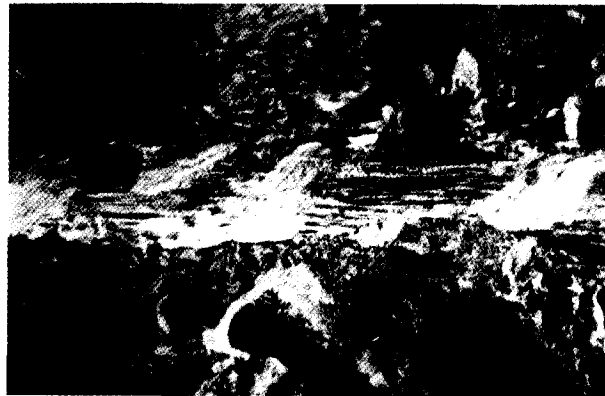

Fig. 2 Pultruded glass rod embedded in concrete after pull-out test.

for several FRP products available in the market place, the surface deformation is an add-on feature manufactured by winding a strand over a pultruded bar before resin curing. A typical example is shown in Fig. 1 for a pultruded glass FRP rod. Fig. 1 compares the rod appearance before testing (top) and after pull-out from a concrete block (bottom). Fig. 2 shows the rod still embedded in concrete at the conclusion of the test. In both pictures, the extent of the damage to the helically wrapped strand is very evident. Also visible is the extensive longitudinal grooving into the resin due to slip over concrete. Clearly, the rigidity of FRP composites (transverse always and longitudinal sometimes) is lower than that of the surrounding concrete. This means that one of the two typical failure modes experienced with conventional steel reinforcing bars, crushing of the concrete between the lugs when the rod slips (Abrishami and Mitchell 1992), is no longer possible when FRP rods are used.

This paper aims to present a simple model to explain the bond mechanism of braided FRP hybrid rods. The model was derived for hybrid-type rods rather than FRP-only rods because experimental work (i.e., concentric pull-out tests) was performed to evaluate the potential of hybrid reinforcement. In this context, a hybrid rod consists of an FRP skin braided directly on a steel

core and fully bonded to it. The rationale for this combination has been explained elsewhere (Nanni, *et al.* 1992, 1994, 1994a). Experimental results on the concentric pull-out tests performed on eleven different types of hybrid rods are given in the literature (Nanni, *et al.* 1997). The proposed analytical model can be used for two major purposes:

1) To compute the transverse tensile stress field in the concrete surrounding the hybrid rod as a result of the rod slip. Knowledge of the stress field allows one to predict the occurrence of split cracking and, therefore, to design for the necessary concrete cover. The proper dimensioning of concrete cover for FRP reinforcement has never been addressed directly, even though there have been unsubstantiated claims that a reduction over the conventional thickness is possible beacause FRP reinforcement does not corrode.

2) To compute the friction coefficient between FRP reinforcement and concrete in order to predict the necessary development length. Up to now, development length requirements for FRP rods have been based solely on the modification of the equations derived for deformed steel reinforcing bars. This is a questionable approach because the bond mechanism and failure modes are different.

2. Model

2.1. Bond mechanism

The tendency of hybrid rods to cause unusual split cracking of the surrounding concrete was evidenced in a study of RC beams where longitudinal cracks occurred at the level of the hybrid reinforcement, with more noticeable damage as the thickness of the FRP skin increased (Nanni, *et al.* 1994a). It was hypothesized that, as the rod slipped, compression of the FRP skin within its original imprint in the concrete was responsible for the cracks. The model proposed herein is based on that concept: compressed FRP creates radial stresses that on one hand provide, through friction, the resistance to slip, but at the same time result in transverse stresses which may cause splitting of the concrete. The experimental study on concentric pull-out has revealed further evidence for this approach (Nanni, *et al.* 1997). As presented in Fig. 3, a close examination of specimens that failed by splitting shows no damage to the concrete surrounding the rod as a result of rod slip. The concrete imprint of the rod is undisturbed, whereas the rod itself shows some minor surface damage. Also evident in Fig. 4 is the gap between the original concrete imprint and the rod in its new compressed position.

2.2. Equivalent shape

In order to derive the relationship between slip, amount of compressed skin, and resulting radial stress field, the actual configuration of the FRP skin was modified to a simpler geometry which maintains the same FRP material volume. The actual shape is made up of interwoven deformations in the form of diamonds (Fig. 5), the simplified shape is made of a series of frustums (Fig. 6). With respect to the simplified shape, values of r_{av}, h, and $s/2$ represent the average radius of the rod, and the height and length of each frustum (Fig. 7). The radial stress field created by the rod onto the concrete, as it slips an amount Δx, is dependent upon the compressed volume of FRP skin (Fig. 8). It can be shown that for any value of Δx, the change

Fig. 3 Undamaged imprint in concrete (specimen H7) and light surface damage to the rod.

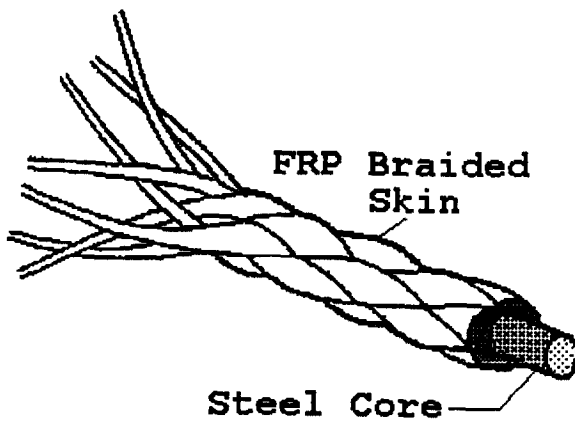Fig. 4 Gap between rod and concrete after slippage (specimen H7).
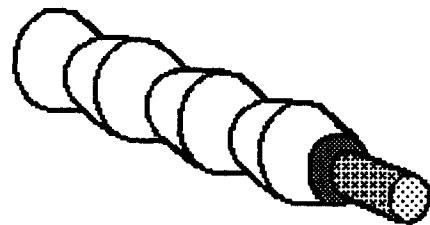

Fig. 5 Braided hybrid rod.
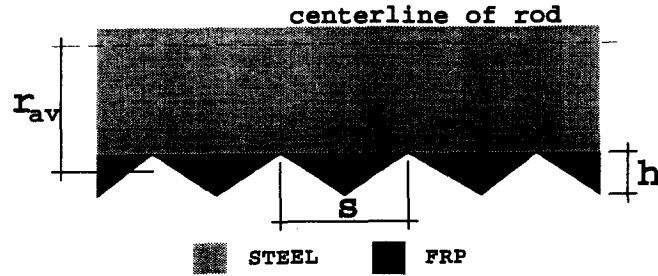

Fig. 6 Simplified hybrid rod.

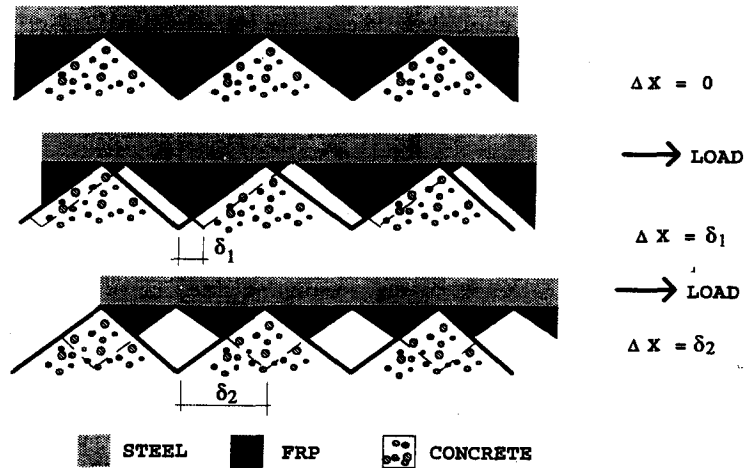Fig. 7 Relevant dimensions for simplified hybrid rod.

Fig. 8 Deformations of FRP skin as a result of slip.

in volume of the frustums can be reduced to that of a cylinder of radius r_{av} where the change in radius Δr_{av} is:

$$\Delta r_{av} = \frac{h}{s^2} \Delta x \, (s - \Delta x) \qquad [mm] \qquad (1)$$

A limitation for the validity of Eq. (1) is that $0 < \Delta x < s/2$.

2.3. Deformability of concrete

As the compressed FRP applies pressure to the concrete, the concrete at the interface also deforms, lessening the deformation of the layer of FRP. The deformation of the concrete can be determined considering the concrete as an elastic system of known geometry and elastic constants. It is found that the deformability of concrete may result in a significant reduction in Δr_{av} depending upon the ratio of the transverse modulus of elasticity of the FRP skin to that of the concrete. This reduction is expressed by a factor defined as k. In order to simplify the computation of k, it was assumed that: a) the deformable layer of concrete corresponds to a layer with thickness equal to h (i.e., the height of the frustum); and, b) the steel core is infinitely rigid with respect to the other two materials (FRP skin and concrete).

2.4. Radial and transverse pressure

Given the effective change in rod radius, $k\Delta r_{av}$, it is possible to compute the radial pressure or stress, σ_{r0}, at the interface between FRP skin and concrete. This radial stress is a function of the transverse modulus of the hybrid rod, $E_{H,t}$. $E_{H,t}$ is a combination of the moduli of individual constituents, i.e., fiber $(E_{F,t})$, resin $(E_{R,t})$, and steel $(E_{S,t})$, based on the volume fraction of each constituent. The formula used for the calculation of $E_{H,t}$ is given below:

$$\frac{1}{E_{H,t}} = \frac{V_F}{E_{F,t}} + \frac{V_R}{E_{R,t}} + \frac{V_S}{E_{S,t}} \qquad [\text{GPa}^{-1}] \tag{2}$$

where the $V's$ are the volume fractions of each material and $V_F + V_R + V_S = 1$. Assuming that the concrete surrounding the bar is shaped like a cylinder with diameter $(2r_2)$ equal to the side of the cube used in the experiment (150 mm), the expressions for radial stress at the FRP-concrete interface and the resulting transverse stress field in concrete, σ_{r0} and σ_{θ}, are defined as follows:

$$\sigma_{r0} = 1000k\frac{\Delta r_{av}}{r_{av}}E_{H,t} \qquad [\text{MPa}] \tag{3}$$

$$\sigma_{\theta} = \frac{\sigma_{r0}r_{av}^2}{r_2^2 - r_{av}^2}\left(1 + \frac{r_2^2}{r^2}\right) \qquad [\text{MPa}] \tag{4}$$

Where r_2 is the outer radius of the concrete cylinder (i.e., 75 mm), r_{av} is the average rod radius and also the inner radius of the concrete hollow cylinder, and r is the radius at which the transverse stress is being evaluated $(r_{av} < r < r_2)$.

2.5. Initiation and propagation of a crack

This section is not necessarily part of the model, but it is needed for the purpose of defining the overall resistance of the concrete cylinder against splitting. The behavior of concrete around the rod can be simulated by a series of concrete rings of arbitrary thickness. The radial pressure applied at r_{av} can be increased by increasing the rod slip until the corresponding transverse stress at FRP-concrete interface reaches the value of the splitting strength, f'_{ct}, of the concrete. At this point, there is the initiation of a radial crack. The radial crack propagates through the thickness of the first concrete ring and relieves the layer of concrete surrounding the rod of any transverse stress. By repeating the process for the adjacent ring and so on, it is possible to re-apply Eq. (4) with: a) σ_{r0} as the radial pressure at the outer diameter of the last cracked ring, and b) the inner radius (r_{av}) equal to the distance from the cylinder center to the last cracked ring. The slip would have to further increase so that the corresponding radial and transverse stresses at the new front increase and become such that the crack propagates to the next adjacent ring. For the geometry and assumptions of this case (i.e., initial inner radius 15 mm, outer radius 75 mm), it can be shown that the value of radial pressure at the FRP-concrete interface required to take the crack through r_2 is close to 4.5 times the radial pressure required for the initiation of the first radial crack. The value $4.5 f'_{ct}$ is defined as the nominal cracking strength of the given concrete specimen and will be used later for comparisons with experimental data.

2.6. Friction

The model, in combination with experimental results from pull-out tests, can be used to derive a nominal coefficient of kinetic friction, μ_k, between the hybrid rod and concrete. Mechanics dictates that $P=\mu_k N$, where P is the pull-out load applied to the rod, and N is the force normal to the rod due to radial pressure. For each value of P, a corresponding value of slip Δx was measured during the tests. Radial pressure is directly related to slip as found in the model. Therefore, N can be found by multiplying the radial pressure, σ_{r0}, by the rod surface area. All factors are known but the coefficient μ_k. In the derivation of μ_k, some assumptions have been made. First, it has been assumed that friction is the only component of bond strength, and second, that friction is uniform along the embedded length of the rod. Third, the embedded length of rod is considered as a rigid body, with the value of the slip constant over the embedment length. Fourth, the free-end movement is chosen to represent the slip of the rod.

3. Comparison with experimental data

The experimental work used for validation of this model is reported elsewhere (Nanni, *et al.* 1997). For this analytical study, only the 19 specimens that failed by splitting of the concrete are reported. Table 1 shows a summary of these data including specimen code (Column 1), rod type (Column 2), concrete compressive strength (Column 8), free-end slip corresponding to maximum load (Column 9), and maximum pull-out load (Column 10). Rods consisted of a steel core of high (SBPR80) or low (SR24) yield strength, and of a skin made of aramid or poly-vinyl alcohol (PVA) FRP. Details regarding constituent material properties and geometry are given in the cited reference. Concrete strengths were 14.4 and 36.2 MPa.

3.1. Radial and transverse pressures

One objective was to compute the radial stress and its corresponding ideal transverse stress at the FRP-concrete interface based on the experimental free-end slip at the time of failure. The ideal transverse stress could then be compared with the overall nominal cracking strength of the sample computed at $4.5\, f_{ct}'$ as from the multiple-ring analogy. The following steps were taken:

— First, the external deformations of the hybrid rods were measured to arrive at suitable dimensions for the simplified equivalent shape of the FRP skin made of frustums. It was found that the length and height of the deformations (diamonds) measured from the rods could be used as values of s and h for the frustums. Columns 3 and 4 in Table 1 show the average dimensions of these diamonds as measured in the laboratory.
— Second, the effect of concrete deformability was computed based on the relative transverse moduli of concrete and FRP skin. Assuming that concrete is homogeneous and using the conventional relationship between compressive strength and modulus of elasticity ("Building" 1989), the rigidity of concrete was derived as 17.79 and 28.46 GPa for the low and high strength respectively. The values of transverse moduli for aramid and PVA FRP skins were not known. Therefore, approximate values of 3.84 and 1.29 GPa were computed based on the moduli of the individual components (i.e., aramid fiber plus resin, and PVA fiber plus

Table 1. Hybrid rod characteristics and pull-out test results (concrete split failure)

										Experimental		Analytical	
Code	Rod type	Diamonds height (mm)	length (mm)	Steel area (mm²)	FRP area (mm²)	$E_{H,t}$ (GPa)	f_c' (MPa)	Free-end slip (mm)	Max. load (kN)	σ_{r0} (MPa)	σ_θ (MPa)
(1)	(2)	(3)	(4)	(5)	(6)	(7)	(8)	(9)	(10)	(11)	(12)
H1-1-a	K48/9 mm/SR24	0.25	20.3	63.6	33	4.96	14.4	1.91	15.76	17.82	17.97
H1-2-a								1.11	16.01	10.81	10.90
H2-1-a	K64/9 mm/SR24	0.50	21.2	63.6	42	4.24	14.4	0.98	15.51	15.35	15.49
H2-2-a								1.90	19.31	24.29	24.51
H3-1-a	K96/9 mm/SR24	0.75	25.6	63.6	65	3.40	14.4	1.08	17.79	16.49	16.65
H3-2-a								0.83	19.57	12.80	12.93
H4-1-a	K64/9.2 mm/SBPR80	0.50	22.9	66.5	42	4.34	14.4	1.50	18.05	21.36	21.56
H4-2-a								0.65	21.35	9.62	9.71
H5-1-a	K96/9.2 mm/SBPR80	0.50	24.3	66.5	65	3.47	14.4	1.29	18.05	14.03	14.16
H5-2-a								1.30	19.83	14.13	14.26
H6-1-a	K96/13 mm/SR24	0.75	31.4	132.7	65	5.11	14.4	1.15	25.42	15.34	15.63
H7-1-a	K96/13 mm/SBPR80	0.75	31.4	132.7	65	5.11	14.4	0.75	22.88	10.14	10.33
H9-1-a	V64/9 mm/SR24	0.50	22.0	63.6	50	2.67	14.4	2.01	18.56	21.71	21.90
H10-1-a	V96/9 mm/SR24	0.75	26.3	63.6	75	2.18	14.4	0.79	13.98	16.94	17.10
H10-2-a								1.51	20.08	9.08	9.17
H7-1-b	K96/13 mm/SBPR80	0.75	31.4	132.7	65	5.11	36.2	2.09	40.61	29.79	30.35
H7-2-b								2.45	48.61	34.49	35.14
H11-1-b	V96/9.2 mm/SBPR80	0.50	24.0	66.5	75	2.22	36.2	3.37	41.52	26.24	26.49
H11-2-b								4.14	48.59	31.04	31.32

$E_{steel} = 200$ GPa; $E_{aramid,t} = 6.90$ GPa; $E_{PVA,t} = 1.50$ GPa; $E_{resin,t} = 0.98$ GPa

resin) (See footnote to Table 1). Based on these values, the reduction factor k could be computed as: 0.78 and 0.93 for aramid and PVA FRP skins in contact with 14.4-MPa concrete, and 0.86 and 0.95 for aramid and PVA FRP skins in contact with 36.2-MPa concrete.

— Third, the values of $E_{H,t}$ were computed on the basis of Eq. (2), knowing the transverse rigidity of constituent materials (See footnote to Table 1) and the volume fractions based on cross-sectional areas (Columns 5 and 6 in Table 1). For simplicity, it was assumed that the FRP skin consists of equal parts of fiber and resin ($V_F = V_R$). Computed values of $E_{H,t}$ are shown in Column 7 of Table 1.

— Fourth, the radial and transverse stresses resulting from Eqs. (3) and (4) were derived for values of a slip Δx equal to the free-end slip recorded at the time of concrete split failure. These stresses are tabulated in Columns 11 and 12 of Table 1.

Assuming that the splitting strength of concrete is determined by the formula $f_{ct}' = 0.26 \, (f_c')^{0.73}$ [MPa] (Carino and Lew 1982), it is possible to predict the nominal concrete strength corresponding to split failure based on the multiple-ring analogy (i.e., 4.5 f_{ct}'). Fig. 9 shows a diagram

where the y-axis represents the ratio of ideal transverse stress (σ_θ) over nominal cracking strength ($4.5 f'_{ct}$), and the x-axis represents the 19 individual specimens. The legend shows that the specimens have been subdivided into four groups according to FRP skin type and concrete strength. There is consistency of results among the four groups, implying that there is no significant influence of concrete strength or FRP skin type on the transverse stress-strength ratio. Overall, the transverse stress-strength ratio varied from a minimum of 1.11 to a maximm of 2.98. This would indicate that the model is conservative.

3.2. Friction coefficient

Experimental data was used in combination with the model to graph the coefficient of friction over slip according to the procedure previously discussed. The trend for the coefficient of friction over slip is shown in Fig. 10 for nine representative specimens (five with the 14.4 MPa concrete and four with the 36.1 MPa concrete). For all specimens, it is evident that the coefficient of
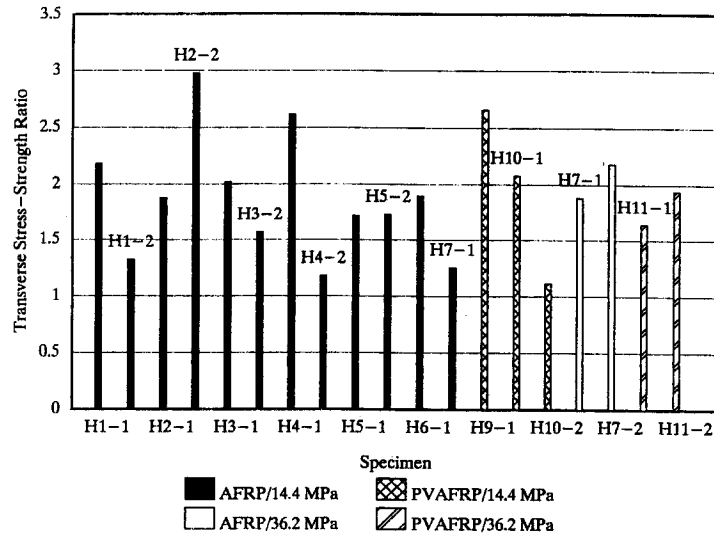

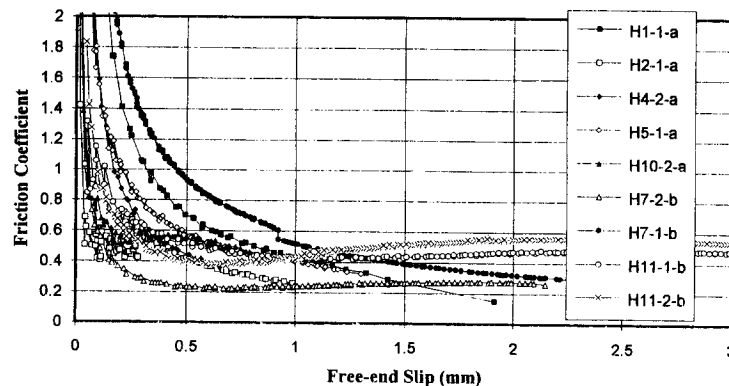Fig. 9 Ideal transverse stress-to-nominal split strength ratio for all specimens.

Fig. 10 Friction coefficient as a function of slip.

friction progressively decreases from infinity to values less than the unity when the slip is anywhere between 0.5 and 1 mm. It then stabilizes at a constant level. This is most evident in the specimens with the higher strength concrete, for which higher values of slip could be attained prior to split failure. For the constant portion of the curves, the PVA rods tend to show higher coefficients of friction than the aramid rods (0.50 to 0.55 as compared to 0.25 to 0.30). This could be confirmed by observing the rod surface after testing and noting that more sever surface damage was caused to the PVA skin.

In the computation of development length that is to follow, it is necessary to adopt a permissible value of slip. Based on Fig. 10 and for the sake of simplicity, it was decided to adopt a slip of 1 mm and a corresponding coefficient of friction equal to 0.40 for all rod types. Although more experimental evidence is necessary to justify such an assumption, this choice allows for the explanation of the procedure.
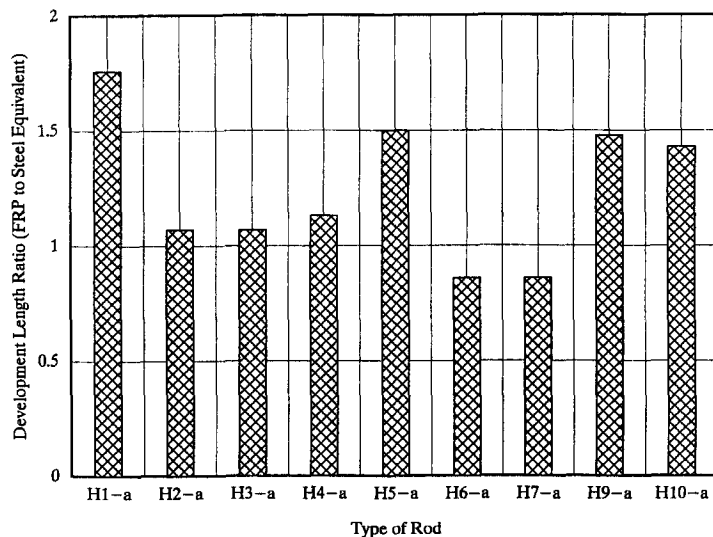

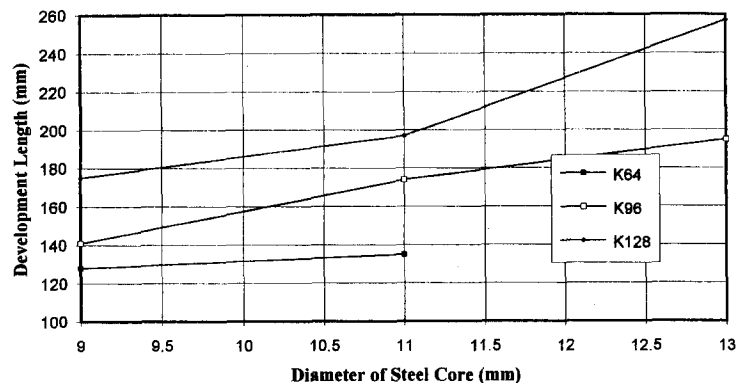Fig. 11 Ratios of transfer lengths/FRP to steel equivalents.

Fig. 12 Development length for hybrid rods as a function of steel core diameter.

3.3. Development length

The coefficient of friction ($\mu_k = 0.40$) is used to calculate the embedment length for each hybrid rod that is necessary to develop the yield capacity when the free-end slip is 1 mm. The development length for each hybrid rod may be compared against the development length of its equivalent deformed steel reinforcing bar (equivalent in terms of total yield force capacity). A Grade 60 steel (420 MPa) was considered for this comparison, along with the ACI 318-89 code formula for the computation of the basic development length in tension (i.e., $0.04 A_b f_y / \sqrt{f_c'}$). Fig. 11 shows the development length ratio of hybrid rod-to-steel equivalent for the case of rods embedded in 14.4 MPa concrete. At the admissible slip of 1 mm, the hybrid rods required from 0.86 to 1.79 times the development length of their steel equivalents.

A theoretical examination of required development lengths is shown in Fig. 12. The figure presents the example of hybrid rods with a SR24 steel core with changes in aramid FRP skin (K64, K96, K128) and steel core diameter (9 to 13 mm). The diagram seems to indicate that the development length increases with skin thickness for identical core sizes. With reference to this figure, the curve relative to the K64 skin is interrupted at a core diameter of 11 mm because it would not be possible to fully encase a larger-size core with the given amount of FRP.

The effect of varying the admissible slip on development length is shown in Fig. 13 for hybrid rods with aramid FRP skin embedded in 14.4 MPa concrete. For the curves herein presented the coefficient of friction was 0.40. As expected, the required development length decreases as the value of admissible slip increases. This diagram is presented only to show the implication of the choice of a slip threshold.

3.4. Design guidelines

The model may also be used to provide design guidelines. Graphs may be compiled to show the relationship between radial pressure at the FRP-concrete interface and free-end slip; radial pressure and development length; and radial pressure and radius of concrete cover required to prevent split failure. Together, these graphs may be used as a design aide as shown in Fig. 14. This figure shows five aramid FRP hybrid rods with two core sizes. For example, a K128/9 mm/SR24 rod may be chosen and allowed 1.5 mm of free-end slip, at which yielding capacity is obtained. The resulting radial pressure at the FRP-concrete interface is 22.6 MPa. This would require a development length of 120 mm, and 106 mm for the radius of concrete cover (or roughly 100 mm or clear cover). The equivalent deformed reinforcing bar in Grade 60 steel would require a development length of 100 mm with a clear cover of 38 mm. This is only a preliminary picture of possible design aides that may be derived from the model. A more significant experimental sample would confirm these findings and provide a more accurate base for such guidelines.

4. Conclusions

It was experimentally found that the bond strength of hybrid rods is roughly equivalent to that of deformed steel reinforcing bars. However, the hybrid rods experience much higher slip.
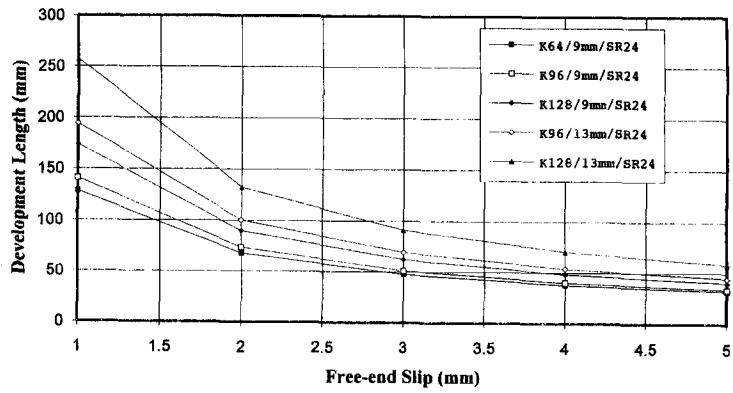
Antonio Nanni and Judy Liu
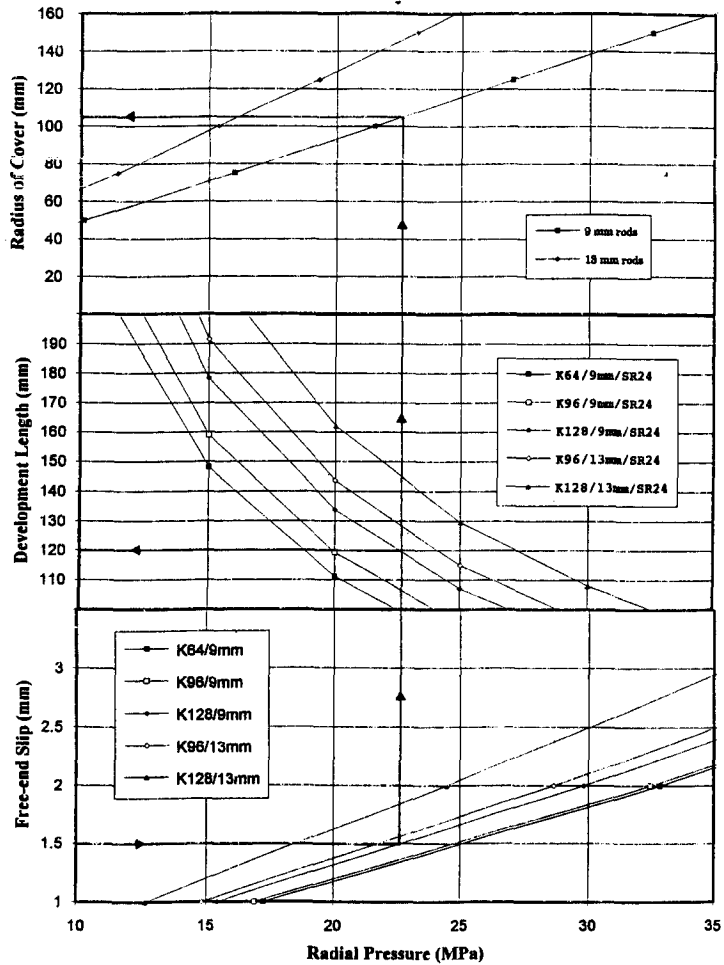

Fig. 13 Development length *vs.* free-end slip.

Fig. 14 Compiled design aide for FRP rods.

For given embedment length, and concrete cover and strength, the pull-out test showed failures either by rod pull-out or splitting the concrete. In both instances there was no evidence of local damage to concrete at the interface FRP-concrete. Given the geometry of the hybrid rod surface deformations and relative rigidity with respect to concrete, there is no crushing of the concrete due to rod slip.

A simple model has been developed to determine radial and transverse stress fields at the interface FRP-concrete. The model is based on a simplified rod geometry and assumes that friction is the only component of bond strength. The model examines the relationship between the slip of the rod and the splitting of the concrete, computing radial and transverse stresses based on the movement of the rod. This model is used to derive the coefficients of friction of the rods and, from here, the required development length. The model seems to indicate that the concrete cover is always larger than that presently required by the code for steel deformed reinforcing bars.

After further experimental verification, this model could be used as a design aide, providing information about the required concrete cover and development length.

Acknowledgements

Notations

A_b	Area of steel reinforcing bar
$E_{H,}$, $E_{F,}$, $E_{R,}$, $E_{S,}$	transverse elastic moduli for hybrid rod, fiber, resion, and steel (GPa)
f_c'	concrete compressive strength
f_{ct}'	concrete splitting strength (MPa)
f_y	Yield strength of steel
h	height of a frustum (mm)
k	reduction factor to account for concrete deformability
N	force resulting from radial pressure (kN)
P	pullout load (kN)
r	concrete radius at which the transverse stress is being evaluated (mm)
r_{av}	average radius of simplified hybrid rod (mm)
r_2	outer radius for concrete cylinder (i.e., 75 mm)
s	twice the length of a frustum (mm)
V_F, V_R, V_S	volume fractions for fiber, resin, and steel (%)
Δr_{av}	change in equivalent rod radius (mm)
Δx	rod slip (mm)
δ_1, δ_2	selected values of rod slip (mm)
σ_{r0}	radial stress at the FRP-concrete interface (MPa)
σ_θ	transverse stress at a radius r (MPa)
μ_k	coefficient of friction

References

Abrishami, H.H. and Mitchell, D. (1992), "Simulation of uniform bond stress", *ACI Materials Journal*, March-April 1992, **89**(2), 161-166.

"Building code requirements for reinforced concrete", (1989), *ACI Committee 318*, American Concrete Institute, Detroit, MI, 347.

Carino, N.J. and Lew, H.S. (1982), "Re-examination of the relation between splitting tensile and compressive strength of normal weight concrete", *ACI Journal*, May-June 1982, **79**(3), 214-218.

Mallik, P.K. (1988), *Fiber-reinforced composites: materials, manufacturing, and design*, Marcel Dekker, Publisher, New York, NY, 469.

Nanni, A., Okamoto, Tanigaki, M. and Henneke, M. (1992), "Hybrid (FRP + Steel) reinforcement for concrete structures", *Proc., ASCE Materials Engineering Congress*, Atlanta, GA, American Society of Civil Engineers, New York, NY, 655-663.

Nanni, A., Henneke, M.J. and Okamoto, T. (1994), "Tensile properties of hybrid rods for concrete reinforcement", *Construction and Building Materials*, **8**(1), 27-34.

Nanni, A., Henneke, M.J. and Okamoto, T. (1994-a), "Behavior of concrete beams with hybrid reinforcement", *Construction and Building Materials*, **8**(2), 89-95.

Nanni, A., J. Nenniger, K. Ash, and J. Liu, (1997), "Experimental bond behavior of hybrid rods for concrete reinforcement", *Structural Engineering and Mechanics, An Int'l Journal*, **5**(4), 339-353.